



## Impact of International Shipping Emissions on Ozone and PM<sub>2.5</sub>: The Important Role of HONO and ClNO<sub>2</sub>

Jianing Dai<sup>1</sup>, Tao Wang<sup>1</sup>

Department of Civil and Environmental Engineering, The Hong Kong Polytechnic University,  
5 Hong Kong, 999077, China

Correspondence to: Tao Wang ([cetwang@polyu.edu.hk](mailto:cetwang@polyu.edu.hk))

**Abstract.** Ocean-going ships emit large amounts of air pollutants such as nitrogen oxide (NO<sub>x</sub>) and particulate matter. Ship-released NO<sub>x</sub> can be converted to nitrous acid (HONO) and nitryl chloride (ClNO<sub>2</sub>), which produce hydroxyl (OH) and chlorine (Cl) radicals and recycle NO<sub>x</sub>,  
10 thus affecting the oxidative capacity and production of secondary pollutants. However, these effects have not been quantified in previous investigations of the impacts of ship emissions. In this study, a regional transport model (WRF–Chem) revised to incorporate the latest HONO and ClNO<sub>2</sub> processes was used to investigate their effects on the concentrations of RO<sub>x</sub>  
15 (RO<sub>2</sub>+HO<sub>2</sub>+OH) radicals, O<sub>3</sub>, and fine particulate matter (PM<sub>2.5</sub>) in Asia during summer. The results show that the ship-derived HONO and ClNO<sub>2</sub> increased the concentration of RO<sub>x</sub> radicals by approximately two to three times in the marine boundary layer. The enhanced radicals then increased the O<sub>3</sub> and PM<sub>2.5</sub> concentrations in marine areas, with the ship contributions increasing from 9% to 21% and from 7% to 10%, respectively. The largest RO<sub>x</sub> enhancement was simulated  
20 over the remote ocean with the ship contribution increasing from 29% to 50%, which led to increases in ship-contributed O<sub>3</sub> and PM<sub>2.5</sub> from 21% to 38% and from 13% to 19%, respectively. In coastal cities, the enhanced levels of radicals also increased the maximum O<sub>3</sub> and averaged PM<sub>2.5</sub> concentrations from 5% to 11% and from 4% to 8% to 4% to 12%, respectively. These findings indicate that modeling studies without considering HONO and ClNO<sub>2</sub> can  
25 significantly underestimate the impact of ship emissions on radicals and secondary pollutants. It is therefore important that these nitrogen compounds be included in future models of the impact of ship emissions on air quality.



## 30 1 Introduction

Exhaust emissions by ocean-going ships affect the chemical compositions of the marine atmosphere and have a significant impact on the climate, air quality, and human health (Andersson et al., 2009; Corbett et al., 2007; Eyring et al., 2010; Liu et al., 2016). The key air pollutants emitted by ship vessels include gases such as sulfur dioxide (SO<sub>2</sub>) and nitrogen oxides (NO<sub>x</sub> = NO + NO<sub>2</sub>) and particulate matter (PM) (Eyring et al., 2005; Moldanová et al., 2009). Emissions of NO<sub>x</sub> and other ozone (O<sub>3</sub>) precursors (volatile organic compounds (VOCs) and carbon monoxide (CO)) from shipping contribute to the tropospheric O<sub>3</sub> burden and hydroxyl radicals (OH), thereby influencing global radiative forcing and oxidative power (Lawrence and Crutzen, 1999). Ship-generated aerosols also affect the radiative budget by scattering and absorbing solar and thermal radiation directly and by altering cloud properties (Devasthale et al., 2006; Eyring et al., 2010; Fuglestvedt et al., 2009; Lawrence and Crutzen, 1999; Liu et al., 2016). Ship emissions in ports and near the coast also influence the air quality of coastal cities (Liu et al., 2018; Zhang et al., 2017c) and threaten public health (Campling et al., 2013; Liu et al., 2016). As international shipborne trade continues to increase, ship emissions are expected to continuously grow at a rate of 3.5% over the 2019-2024 period (UNCTAD, 2019), and their impact on the environment is a growing concern.

The effects of ship emissions on the formation of O<sub>3</sub> and PM<sub>2.5</sub> have been extensively evaluated in numerical studies. On the open ocean, ship-generated NO<sub>x</sub> reacts with VOCs emitted from ships and from the background atmosphere and enhances O<sub>3</sub> formation (Aksoyoglu et al., 2016; Corbett and Fischbeck, 1997; Huszar et al., 2010; Hoor et al., 2009; Lawrence and Crutzen, 1999). In coastal areas, the O<sub>3</sub> levels can also be increased by NO<sub>x</sub> emitted from ships in ports and harbors and through the dispersion of ship-formed O<sub>3</sub> on the open ocean (Aksoyoglu et al., 2016; Song et al., 2010; Wang et al., 2019). On the other hand, ship-generated NO<sub>x</sub> can reduce ozone formation via a titration effect in heavy-traffic ports and within the ship tracks (Aksoyoglu et al., 2016; Wang et al., 2019). Ship emissions have also been shown to increase PM<sub>2.5</sub> concentrations via direct emissions and via the production of secondary aerosols through the reaction of gaseous precursors (Aksoyoglu et al., 2016; Liu et al., 2018; Lv et al., 2018). Although the formation of O<sub>3</sub> and secondary aerosols is affected by their precursors, it can also



be influenced by the levels of radicals, which are key to the oxidation of precursors. Limited  
60 attention has been paid to the production of ship-related radicals in evaluating the effects of ship  
emissions on secondary pollutants.

Recent studies have demonstrated the potentially important roles of two radical precursors and  
nitrogen reservoirs—nitrous acid (HONO) and nitryl chloride (ClNO<sub>2</sub>)—in the atmospheric  
oxidation chemistry (Fu et al., 2019; Li et al., 2016; Sarwar et al., 2014; Simon et al., 2009;  
65 Zhang et al., 2017b). HONO is emitted directly in combustion and soil (Kleffmann et al., 2005)  
or produced by heterogeneous reactions of NO<sub>2</sub> on various surfaces (Finlayson-Pitts et al., 2003;  
Monge et al., 2010; Ndour et al., 2008) and by photolysis of nitrate aerosol (Ye et al., 2016; Ye  
et al., 2017). ClNO<sub>2</sub> is formed from reactions of N<sub>2</sub>O<sub>5</sub>, which is produced when NO<sub>2</sub> reacts with  
O<sub>3</sub>, on chloride-containing aerosol at night (Bertram and Thornton, 2009). Photolysis of HONO  
70 and ClNO<sub>2</sub> by sunlight produces OH or Cl radicals and recycles NO<sub>2</sub>, hence affecting the  
oxidation capacity and production of secondary pollutants (Osthoff et al., 2008; Wang et al.,  
2016). Ships can directly emit HONO (Sun et al., 2020), and their emitted NO<sub>x</sub> can produce  
HONO and ClNO<sub>2</sub> via heterogeneous reactions on sea-salt and ship-emitted particles. Although  
the production and effects of HONO and ClNO<sub>2</sub> from land-based emissions have been  
75 demonstrated over land areas (Zhang et al., 2017a), few studies have examined the effects of the  
two reactive nitrogen species from international shipping. Field studies have observed elevated  
mixing ratios of HONO (0.2 ppb) at a marine site of the Bohai rim in northern China (Wen et al.,  
2019) and of HONO (126 ppt) and ClNO<sub>2</sub> (1.97 ppb) at a coastal site in southern China (Tham et  
al., 2014; Zha et al., 2014). These observations suggest the significant contribution of ship  
80 emissions to the oxidative capacity of the marine and coastal atmosphere in East Asia.

In this study, we used a revised regional chemical transport model to simulate the spatial  
distributions of HONO and ClNO<sub>2</sub> produced by ocean-going ships and their effects on the  
formation of O<sub>3</sub> and PM<sub>2.5</sub> in East Asia, which has 8 of the world's top 10 container ports and the  
world's most trafficked oceans. We selected the summer (July) of 2018 as the study period,  
85 when the summer monsoonal wind prevails in Asia; together with the highest radiation and  
temperature, it has the greatest impact on shipping during the year. We describe in Section 2 the  
details of the model setting, emissions, numerical experiments, observational data, and model  
validation. In Section 3, we exhibit the model performance for HONO and ClNO<sub>2</sub> and compare



the results with available measurements in marine areas; we then show the formation of ship-  
90 related HONO and ClNO<sub>2</sub> and their subsequent effects on radicals, O<sub>3</sub>, and PM<sub>2.5</sub> in oceanic  
areas and coastal cities. Our conclusions are given in Section 4.

## 2. Methodology

### 95 2.1 Model Setting

In this study, the WRF–Chem model (version 3.6.1; Grell et al., 2005) with updated gases-phase  
and heterogeneous-phase mechanisms of new reactive nitrogen species (Zhang et al., 2017a) was  
used to simulate the transport, mixing, and chemical transformation of trace gases and aerosols.  
Briefly, the updated module was based on the default CBMZ module (Zaveri and Peters, 1999),  
100 in which the O<sub>3</sub> production came from the traditional photochemical mechanisms with only two  
gas-phase sources of HONO (OH+NO → HONO and HO<sub>2</sub> + NO<sub>2</sub> → HONO) and no chlorine  
chemistry. In the updated module (CBMZ-ReNOM), the HONO sources included the additional  
gas-phase reactions between NO<sub>x</sub> and HO<sub>x</sub> (OH+HO<sub>2</sub>), the heterogeneous reaction of NO<sub>2</sub> on the  
particle, urban, leaf (Kurtenbach et al., 2001), and sea surfaces (Zha et al., 2014), and direct  
105 emission from vehicles (Gutzwiller et al., 2002; Kurtenbach et al., 2001; Sun et al., 2020). For  
this study, an additional HONO source from the photolysis of particulate nitrate was added to our  
model. For ClNO<sub>2</sub> production, the parameterization from Bertram and Thornton (2009) was used  
to represent the N<sub>2</sub>O<sub>5</sub> uptake coefficient and ClNO<sub>2</sub> production yield. This parameterization  
reproduced the order of magnitude and variation of the observed N<sub>2</sub>O<sub>5</sub> and ClNO<sub>2</sub> levels in a  
110 background site of Hong Kong (Dai et al., 2020). The other six chlorine species, with relevant  
photolysis reactions and subsequent reactions between released Cl radical and VOCs, were also  
added to the default module (Zhang et al., 2017a). The details of other chemical and physical  
schemes for the simulation can be found in Zhang et al. (2017a).

The model simulations were performed from June 28 to July 31, 2018. The first 72 h of the  
115 simulations were considered as a spin-up time. The initial meteorological conditions were  
provided by reanalysis data from the final (FNL) Operational Global Analysis dataset provided  
by the National Centers for Environmental Prediction (NCEP);



120 <http://rda.ucar.edu/datasets/ds083.2/>). The model had 31 vertical layers with a fixed top of 100 hPa. The domain covered a large part of Asia with a horizontal resolution of  $36 \times 36$  km (Figure 1a). The surface layer was 30 m above the ground, and the lowest 11 layers were approximately within the height of the planetary boundary layer at noon.

## 2.2 Emissions

Five sets of emission inventories (EIs) were used for anthropogenic emissions in our study. For 125 mainland China, the Multi-resolution Emission Inventory for China (MEIC; <http://www.meicmodel.org/>) in 2016 was used. For the rest of Asia, we applied the MIX (<http://www.meicmodel.org/dataset-mix>) for 2010 (Li et al., 2017). For international shipping, the emission database in the Community Emission Data System (CEDS) (McDuffie et al., 2020) for 2017 was used. The HONO emissions from land transportation sources were calculated using 130 land-based  $\text{NO}_x$  emissions and the HONO/ $\text{NO}_x$  ratios (0.8% for gasoline and 2.3% for diesel). For ship-emitted HONO, we set the emission ratio of HONO/ $\text{NO}_x$  as 0.51% based on the reported ratio in fresh ship plumes in Chinese waters (Sun et al., 2020). For anthropogenic chloride emissions, the high-resolution ( $0.1^\circ \times 0.1^\circ$ ) EIs of HCl and fine particulate  $\text{Cl}^-$  for 2014 were applied for mainland China (Fu et al., 2018). These EIs included four sectors and have been 135 shown to offer a reasonable model simulation of particulate chloride by the WRF-Chem model (Dai et al., 2020). The Reactive Chlorine Emission Inventory (RCEI; Keene et al., 1999) was used for anthropogenic chloride emissions in the other regions. For natural emissions, the biogenic emissions were calculated by the Model of Emission of Gas and Aerosols from Nature (MEGAN) version 2.1 (Guenther et al., 2006).

140 The spatial distribution of ship  $\text{NO}_x$  emissions is shown in Figure 1a. The main ship routes with high emission intensity are clearly identified in the ship emission inventory. One major shipping lane is located in the Southern Bay of Bengal (BOB) in the Indian Ocean, passes through the Strait of Malacca, and extends to the South China Sea (SCS) and other Asian countries. Distinct shipping lanes are also shown along the coast of the East China Sea (ECS) and the Sea of Japan 145 (SOJ). Over the West Pacific Ocean (WPO), congested ship routes are distributed among Japan and other countries (Southeast Asian countries, Australia, and North America). Based on the



distribution of ship  $\text{NO}_x$  emissions, six water zones were selected, including three waters around China (SCS, ECS, Bohai Rim (BR)), two waters in other regions (SOJ and BOB), and one open ocean (WPO; Figure 1b). In addition, three densely populated city clusters were chosen (the  
150 North Central Plain (NCP), the Yangtze River Delta (YRD), and the Pearl River Delta (PRD)).

### 2.3 Experimental Setting

Eight simulations were conducted with different emissions and chemistry, as listed in Table 1. In the Def and Def\_noship cases, the WRF–Chem model was conducted with default chemistry  
155 (i.e., the default CBMZ mechanism with only the two HONO sources and no chlorine chemistry). The differences between Def and Def\_noship (i.e., Def-Def\_noship) represent the effects of ship emissions with the default nitrogen chemistry. In the Cl and Cl\_noship cases, an updated chlorine chemistry in the revised WRF–Chem model was used. The differences between the two cases (i.e., Cl-Cl\_noship) represent the effects of ship emissions with the default and  
160 additional chlorine chemistry. Similarly, in the HONO and HONO\_noship cases, the additional HONO chemistry was used, and the difference between the two cases (i.e., HONO-HONO\_noship) represents the default impact of ship emissions with additional HONO chemistry. In the BASE and BASE\_noship cases, the integrated HONO and chlorine chemistry are considered. The differences between BASE and BASE\_noship represent the shipping impact  
165 with the integrated effects of HONO and chlorine species. The results from the BASE experiment will be used to validate the model performance.

### 2.4 Observational Data and Model Validation

Meteorological data from surface stations from NOAA’s National Climatic Data Center (NCDC;  
170 Figure S1a) comprising wind direction, wind speed, surface temperature, and specific humidity were used to validate model performance for the meteorological parameters. Conventional air pollutant data ( $\text{NO}_2$ ,  $\text{PM}_{2.5}$ , and  $\text{O}_3$ ) from surface stations (obtained from China’s Ministry of Ecology and Environment; Figure S1b) were used to evaluate the simulated air pollutants over China’s land areas. Table S2 summarizes the statistical performance of our model results. For  
175 meteorological parameters, high R values ( $>0.85$ ) and low mean bias (MB) indicate good



performance for the meteorological field. For regular air pollutants, the model overpredicted  $\text{PM}_{2.5}$  ( $\text{MB} = 10.6 \mu\text{g m}^{-3}$ ) and slightly underpredicted  $\text{NO}_2$  ( $\text{MB} = 3.3 \text{ ppbv}$ ) and  $\text{O}_3$  ( $\text{MB} = 5.5 \text{ ppbv}$ ). These biases in simulation can be partially explained by uncertainties in the model input, such as the land-use data (Dai et al., 2019) and emission inventory (Li et al., 2017).

180 The  $\text{O}_3$  data from two remote sites (Ryori and Yonagunijima (Yona)) in Japan  
(<https://www.data.jma.go.jp/ghg/kanshi/ghgp/o3>) and one coastal background site in Hong Kong  
(Hok Tsui (HT)) were used to compare the model performance over the maritime areas. These  
three sites are located along the coasts of the SCS, ECS, and WPO regions (Figure 1b). As  
shown in Figure S2, with the default chemistry, the model underpredicted the  $\text{O}_3$  mixing ratio at  
185 the coastal and marine sites, with underestimation by 2.8, 4.8, and 2.3 ppbv at the HT, Ryori, and  
Yona sites, respectively (Table S3). With the addition of the HONO and  $\text{ClNO}_2$  chemistry, the  
simulated  $\text{O}_3$  levels at the marine sites were improved, with the MB from  $-2.8$  to  $-1.5$  ppbv at  
the HT site,  $-3.0$  to  $-2.3$  ppbv at the Ryori site, and  $-2.3$  to  $-0.7$  ppbv at the Yona site.

## 190 **3 Results**

### **3.1 Simulated HONO and $\text{ClNO}_2$ and Contributions from Ship Emissions**

Figure 2a shows the horizontal distribution of the average HONO at the surface layer in the  
BASE case. The predicted HONO was widespread over the oceans, with mixing ratios ranging  
195 from 0.005 to 0.300 ppbv and distinct higher concentrations along the main shipping lanes. The  
distribution of HONO was consistent with that of  $\text{NO}_2$  (Figure S3) due to the homogeneous and  
heterogeneous conversion of  $\text{NO}_2$  to form HONO. In the vertical direction, the simulated HONO  
was concentrated at the surface and reached up to 400 to 600 m in the coastal and marine areas  
(see Figure S4). Figure 3 shows the vertical profile of HONO from ship emissions in the nine  
200 selected regions. Consistent with the overall HONO vertical distribution, ship-contributed  
HONO also peaked at the surface in the oceanic areas, with average HONO levels of 3 to 120  
pptv in the MBL. The greatest contribution of ship emissions was simulated in the WPO (96%),  
followed by the SOJ (80%), the BOB (49%), three Chinese waters (14% to 16%), and the coastal



cities (3% to 12%). The varying ship contributions in these regions can be explained by the  
205 relative strength of the emissions from ships and from the adjacent land areas.

High values of  $\text{ClNO}_2$  were simulated along the coasts and peaked in the lower MBL (Figure  
2b), with mixing ratios ranging from 2 to 400 pptv in oceanic areas and the highest value in the  
BR region. This distribution was in line with that of its precursors  $\text{N}_2\text{O}_5$  (Figure S5) and  
particulate chloride (Figure S6). Vertically, the peak value of  $\text{ClNO}_2$  was simulated in the  
210 residual layer (100 to 300 m; Figure 3), with mixing ratios of 8 to 350 pptv in oceanic areas.  
Similar to HONO, the greatest ship contribution to  $\text{ClNO}_2$  was also simulated in the WPO  
(61%), followed by other oceanic areas (9% to 24%) and coastal cities (5% to 11%).

We compared the modeled HONO and  $\text{ClNO}_2$  with field observations made at some coastal and  
marine sites (see Table S4). The simulated HONO mixing ratios were 0.1 to 0.3 ppbv and 0.01 to  
215 0.1 ppbv over BR and SCS, respectively, which were comparable with the measurements at the  
marine sites of BR (0.2 ppbv) (Wen et al., 2019) and SCS (89 pptv) (Table S4). For the coastal  
areas of other Asian countries, the simulated HONO compared well with the measurements in  
South Korea (0.60 ppbv) (Kim et al., 2015) and Japan (0.63 ppbv) (Takeuchi et al., 2013).  
HONO was simulated at approximately 5 pptv in the open ocean and 10 to 25 pptv along the  
220 main shipping lanes (Figure 2a), which were comparable to the measured HONO (3 to 35 pptv)  
in the open ocean in Europe and North America (Kasibhatla et al., 2018; Meusel et al., 2016; Ye  
et al., 2016). For  $\text{ClNO}_2$ , the order of magnitude and variation of the measured  $\text{N}_2\text{O}_5$  and  $\text{ClNO}_2$   
levels at the HT site have been reasonably reproduced by our model for early autumn of 2018  
(Dai et al., 2020). The model performance of HONO and  $\text{ClNO}_2$  in the land areas of mainland  
225 China for the summer of 2014 was also evaluated by Zhang et al. (2017). Overall, our model  
ability in simulation of HONO and  $\text{ClNO}_2$  is acceptable, and the model results are sufficiently  
reliable for further analysis.

### 3.3 Impact of Ship-Derived HONO and Chlorine on $\text{RO}_x$ , $\text{O}_3$ , and $\text{PM}_{2.5}$



230 In this section, we evaluate the ship effects on the main atmospheric radicals ( $\text{RO}_x$ ,  
 $\text{OH}+\text{HO}_2+\text{RO}_2$ ),  $\text{O}_3$ , and  $\text{PM}_{2.5}$  with the default chemistry (described in Section 2.3) and with the  
additional HONO and chlorine chemistry.

### 3.3.1 $\text{RO}_x$

235 Figure 4 shows the simulated differences in the average daytime  $\text{RO}_x$  mixing ratios at the surface  
from the cases with and without ship emissions using different chemistry. The  $\text{RO}_x$  mixing ratio  
was noticeably increased by ship emissions over oceanic areas, and this enhancement was  
magnified by the additional nitrogen chemistry. With the default chemistry (Figure 4a), the  
average ship contribution to  $\text{RO}_x$  was about 18% over the whole oceanic area. The addition of  
240 the HONO and chlorine chemistry increased the ship contributions to 28% (Figure 4b) and 22%  
(Figure 4c), respectively. Photolysis of ship-generated HONO and  $\text{ClNO}_2$  released radicals ( $\text{OH}$   
and  $\text{Cl}$ ; Figure S7) and recycled  $\text{NO}_x$ , which then oxidized VOCs and gave rise to high levels of  
 $\text{RO}_x$ . With the combined HONO and chlorine chemistry, the ship contribution was further  
increased to 38% (Figure 4d). This combined ship contribution was smaller than the sum of that  
245 from the separate HONO and chlorine chemistry ( $22\% + 28\% = 50\%$ ), which can be explained  
by the nonlinear interactions of the chemical system. Figure 5 shows the vertical profile of the  
 $\text{RO}_x$  mixing ratio from ship emissions in the nine regions. The enhanced  $\text{RO}_x$  reached an altitude  
of greater than 2 km over the oceanic regions, indicating the significant impact of ship-derived  
HONO and  $\text{ClNO}_2$  on the oxidative capacity in the marine troposphere.

250 The largest increase in the ship contribution to  $\text{RO}_x$  was predicted in the WPO region (from 29%  
to 50%; Figure 9a), followed by other oceanic areas (from 3% to 12% to 6% to 17%) and coastal  
cities (from -2% to 3% to 4% to 6%). The maximum ship contribution in the WPO region was  
consistent with the greatest ship contribution to HONO and  $\text{ClNO}_2$  in this region (Figure 4d). In  
the SCS and BOB regions, the enhanced  $\text{RO}_x$  was more dispersed with the combined nitrogen  
255 chemistry than that with the default and separate nitrogen chemistry. In the coastal cities, the  
 $\text{RO}_x$  mixing ratio was also affected by ship emissions via the transport of ship-generated HONO  
and  $\text{ClNO}_2$  by summertime winds.



### 3.3.2 O<sub>3</sub>

260 Figure 6 shows the simulated differences in the average O<sub>3</sub> at the surface from the cases with and  
without ship emissions. Consistent with the impact of ship emissions on oceanic RO<sub>x</sub>, the  
oceanic O<sub>3</sub> was also noticeably increased (by 9%) by ship emissions, which was further  
enhanced by the addition of HONO (12%) and ClNO<sub>2</sub> (14%) and combined nitrogen chemistry  
(21%). The simulated distribution of ship-enhanced O<sub>3</sub> with the default chemistry was along the  
265 main shipping routes with high NO<sub>x</sub> emissions (Figure 6a). O<sub>3</sub> formation was highly sensitive to  
NO<sub>x</sub> from ship emissions due to the relatively low concentrations of NO<sub>x</sub> in the marine areas.  
The larger ship contribution with ClNO<sub>2</sub> chemistry than with HONO chemistry may be partially  
explained by a higher production ozone efficiency by NO<sub>2</sub> than by NO (from photolysis of  
HONO) and by the faster reaction rate of Cl radicals than OH radicals with long-lived alkanes.

270 With the combined impact from HONO and ClNO<sub>2</sub>, widespread ozone increases were simulated  
over the SCS, BOB, and WPO regions (Figure 6d). The combined nitrogen chemistry also  
increased the ozone concentrations in the coastal areas; in contrast, these concentrations were  
decreased by HONO or ClNO<sub>2</sub> separately. As shown in Figure 6b and c, distinct ozone  
enhancement was simulated over the marine area of South Korea and Japan by HONO or ClNO<sub>2</sub>.

275 However, this enhancement was weakened and even canceled by their combined effects. We  
calculated an indicator of the ozone formation regimes based on the ratio of the production rate  
of H<sub>2</sub>O<sub>2</sub> to that of HNO<sub>3</sub> (P<sub>H<sub>2</sub>O<sub>2</sub></sub>/P<sub>HNO<sub>3</sub></sub>) (Fu et al., 2020; Zhang et al., 2009). Figure 7, with the  
combined HONO and ClNO<sub>2</sub> chemistry, shows that the NO<sub>x</sub>-sensitive regime in east Asia was  
changed to a VOC-sensitive regime, which was probably due to the increase level of NO or NO<sub>2</sub>

280 from photolysis of HONO.

Figure S8 shows the vertical profile of ship-generated O<sub>3</sub> enhancement in the nine regions.  
Similar to ship-enhanced RO<sub>x</sub>, ship-related O<sub>3</sub> enhancement stretched from the surface to the  
lower troposphere (>2 km) over the marine regions. Because the emissions from ships occur at  
the sea surface, the vertically enhanced O<sub>3</sub> formation was caused by strong convection (Dalsøren  
285 et al., 2009)



The ship contribution to O<sub>3</sub> formation was also simulated in the WPO region (from 21% to 38%; Figure 9b). In other oceanic areas, the contributions of ship emissions were also increased from 3% to 18% to 12% to 24%, with two distinct O<sub>3</sub> enhancements over the BR (~10 ppbv; Figure 6d) and ECS (15 ppbv) regions. In the three coastal city clusters, the reduced O<sub>3</sub> formation was simulated by ship emissions with the default chemistry (from -5 to -1 ppb). Because these coastal cities are in the VOCs-limited regime (Figure 7a), the NO<sub>x</sub> from ships would lead to a decrease in chemical O<sub>3</sub> production. With the combined HONO and ClNO<sub>2</sub> effects, the ship-induced O<sub>3</sub> increased to -1 to -5 ppb due to the enhanced radicals and the transport of O<sub>3</sub> in the marine areas by ship-generated HONO and ClNO<sub>2</sub>. The maximum O<sub>3</sub> increase in coastal cities also doubled from 3 ppb (5%) to 7 ppb (11%), aggravating the negative effects of ship emissions on human health in coastal cities.

### 3.3.3 PM<sub>2.5</sub>

Ship-derived HONO and ClNO<sub>2</sub> also influence the production of aerosols via changes in radicals and NO<sub>x</sub>. Figure 8 shows the simulated differences in the average PM<sub>2.5</sub> at the surface for cases with and without ship emissions. The PM<sub>2.5</sub> concentration was considerably enhanced by ship emissions, and the additional nitrogen chemistry further increased the simulated PM<sub>2.5</sub> concentration. With the default chemistry, the average ship contribution to the PM<sub>2.5</sub> concentration was about 7% in oceanic areas (Figure 8a), and it was increased to 10% with the addition of HONO and ClNO<sub>2</sub> chemistry (Figure 8d). The greatest contribution from shipping to the PM<sub>2.5</sub> concentration was also simulated over the WPO region, as with ozone, with the contribution ranging from 13% with the default chemistry to 19% with the improved chemistry (Figure 9c). In other oceanic areas, the ship contributions were also increased from 2% to 12% to 6% to 15%. We calculated the effects of ship-generated HONO and ClNO<sub>2</sub> on the formation of secondary particles. The additional ship HONO and chlorine chemistry increased the ship contribution to particulate nitrate from 13% to 41% in oceanic areas (Figure S9 and Figure S11) and its contribution to particulate sulfate from 11% to 34% (Figure S10 and Figure S11). In the coastal cities, the default contribution by ships was about 4% to 8%, which was also increased to 4% to 12% with the improved chemistry (Figure 9c). The considerable increase in ship-



315 contributed  $\text{PM}_{2.5}$  and ozone due to HONO and  $\text{ClNO}_2$  demonstrates the need to consider these  
compounds in evaluations of the impact of shipping on air quality.

Previous studies have evaluated the impact of ship emissions on the formation of  $\text{O}_3$  and  $\text{PM}_{2.5}$ .  
Aksoyoglu et al. (2016) simulated the average ship contribution to oceanic  $\text{O}_3$  as 10% to 20% in  
the Mediterranean area, and Huszar et al. (2010) showed a ship contribution of 10% over the  
320 Eastern Atlantic. The maximum  $\text{O}_3$  enhancement by ship emissions was 15 ppb in the coastal  
waters of South Korea (Song et al., 2010) and 30 to 50  $\mu\text{g m}^{-3}$  off the coast of the YRD region  
(Wang et al., 2019). For  $\text{PM}_{2.5}$ , the average ship contributions were about 20% to 25% in  
European waters (Aksoyoglu et al., 2016) and 2.2% to 18.8% off the coast of China (Lv et al.,  
2018).

325 Compared to previous studies, our study simulated a higher contribution to average ozone  
formation and a smaller contribution to average  $\text{PM}_{2.5}$ . However, it is difficult to discern the  
differences in these modeling studies due to the differences in the methodologies adopted,  
including ship emission inventory, model resolution, chemical mechanisms (in addition to  
different treatment of HONO and  $\text{ClNO}_2$  chemistry), and period of study. All studies  
330 demonstrate an important impact of ship emissions on atmospheric chemistry and air quality.  
The key finding of our study is the role of HONO and  $\text{ClNO}_2$  in driving the oxidation processes,  
which has not been fully considered in most previous model studies of the impact of shipping on  
pollutant levels.

#### 335 **4 Conclusions**

This study evaluated the production of HONO and  $\text{ClNO}_2$  from international shipping and their  
impact on the oxidative capacity, ozone level, and level of fine PM in the maritime and coastal  
areas of eastern Asia. The results show that photolysis of the two compounds releases OH and Cl  
radicals, recycles  $\text{NO}_x$ , and increases conventional hydroxyl and organic peroxy radicals ( $\text{RO}_x =$   
340  $\text{OH} + \text{HO}_2 + \text{RO}_2$ ) by 0.8% to 21.4%,  $\text{O}_3$  by 5.9% to 16.6%, and  $\text{PM}_{2.5}$  by 3.2% to 8.6% at the  
surface in coastal and Western Pacific regions. Their impact extends to the marine boundary  
layer. The largest contributions of HONO and  $\text{ClNO}_2$  occur in the relatively remote oceans.  
Because ocean-going ships are a major source of  $\text{NO}_x$ , which is the key chemical precursor to



HONO and ClNO<sub>2</sub>, it is important to consider the sources and chemistry of these nitrogen  
345 compounds in evaluations of the impact of ship emissions.

**Code and data availability.** The codes and data used in this study are available upon request  
from Tao Wang ([cetwang@polyu.edu.hk](mailto:cetwang@polyu.edu.hk)).

350 **Author contributions.** TW initiated the research, and JD and TW designed the paper  
framework. JD ran the model, processed the data, and made the plots. JD and TW analyzed the  
results and wrote the paper.

**Acknowledgments.** We would like to thank Qiang Zhang from Tsinghua University for  
355 providing the emission inventory and Xiao Fu from The Hong Kong Polytechnic University for  
providing the code of HONO sources and anthropogenic chloride emission inventory.

**Financial support.** This research has been supported by the Hong Kong Research Grants  
Council (grant no. T24-504/17-N) and the National Natural Science Foundation of China (grant  
360 no. 91844301).

## References

- Aksoyoglu, S., Baltensperger, U., & Prévôt, A. S. (2016). Contribution of ship emissions to the  
365 concentration and deposition of air pollutants in Europe. *Atmospheric Chemistry &  
Physics*, *16*, 1895–1906.
- Andersson, C., Bergström, R., & Johansson, C. (2009). Population exposure and mortality due to  
regional background PM in Europe—Long-term simulations of source region and shipping  
contributions. *Atmospheric Environment*, *43*, 3614–3620.
- 370 Bertram, T., & Thornton, J. (2009). Toward a general parameterization of N<sub>2</sub>O<sub>5</sub> reactivity on  
aqueous particles: The competing effects of particle liquid water, nitrate and chloride.  
*Atmospheric Chemistry & Physics*, *9*, 8351–8363.
- Campling, P., Janssen, L., Vanherle, K., Cofala, J., Heyes, C., & Sander, R. (2013). Specific  
evaluation of emissions from shipping including assessment for the establishment of



- 375 possible new emission control areas in European Seas. *Flemish Institute for  
Technological Research (VITO), Mol, BE.*
- Corbett, J. J., & Fischbeck, P. (1997). Emissions from ships. *Science*, 278, 823–824.
- Corbett, J. J., Winebrake, J. J., Green, E. H., Kasibhatla, P., Eyring, V., & Lauer, A. (2007).  
Mortality from ship emissions: A global assessment. *Environmental Science &  
380 Technology*, 41, 8512–8518.
- Dai, J., Liu, Y., Wang, P., Fu, X., Xia, M., & Wang, T. (2020). The impact of sea-salt chloride  
on ozone through heterogeneous reaction with N<sub>2</sub>O<sub>5</sub> in a coastal region of south China.  
*Atmospheric Environment*, 117604.
- Dai, J., Wang, X., Dai, W., & Chang, M. (2019). The impact of inhomogeneous urban canopy  
385 parameters on meteorological conditions and implication for air quality in the Pearl River  
Delta region. *Urban Climate*, 29, 100494.
- Dalsøren, S. B., Eide, M., Endresen, Ø., Mjelde, A., Gravir, G., & Isaksen, I. S. (2009). Update  
on emissions and environmental impacts from the international fleet of ships: The  
contribution from major ship types and ports. *Atmospheric Chemistry & Physics*, 9,  
390 e2194.
- Devasthale, A., Krüger, O., & Graßl, H. (2006). Impact of ship emissions on cloud properties  
over coastal areas. *Geophysical Research Letters*, 33.
- Eyring, V., Isaksen, I. S., Berntsen, T., Collins, W. J., Corbett, J. J., Endresen, O., Grainger, R.  
G., Moldanova, J., Schlager, H., & Stevenson, D. S. (2010). Transport impacts on  
395 atmosphere and climate: Shipping. *Atmospheric Environment*, 44, 4735–4771.
- Eyring, V., Köhler, H., Van Aardenne, J., & Lauer, A. (2005). Emissions from international  
shipping: 1. The last 50 years. *Journal of Geophysical Research: Atmospheres*, 110.
- Finlayson-Pitts, B., Wingen, L., Sumner, A., Syomin, D., & Ramazan, K. (2003). The  
heterogeneous hydrolysis of NO<sub>2</sub> in laboratory systems and in outdoor and indoor  
400 atmospheres: An integrated mechanism. *Physical Chemistry Chemical Physics*, 5, 223–  
242.
- Fu, X., Wang, T., Gao, J., Wang, P., Liu, Y., Wang, S., Zhao, B., & Xue, L. (2020). Persistent  
heavy winter nitrate pollution driven by increased photochemical oxidants in northern  
China. *Environmental Science & Technology*, 54, 3881–3889.



- 405 Fu, X., Wang, T., Wang, S., Zhang, L., Cai, S., Xing, J., & Hao, J. (2018). Anthropogenic emissions of hydrogen chloride and fine particulate chloride in China. *Environmental Science & Technology*, *52*, 1644–1654.
- Fu, X., Wang, T., Zhang, L., Li, Q., Wang, Z., Xia, M., Yun, H., Wang, W., Yu, C., & Yue, D. (2019). The significant contribution of HONO to secondary pollutants during a severe  
410 winter pollution event in southern China. *Atmospheric Chemistry and Physics*, *19*, 1–14.
- Fuglestvedt, J., Berntsen, T., Eyring, V., Isaksen, I., Lee, D. S., & Sausen, R. (2009). *Shipping emissions: From cooling to warming of climate and reducing impacts on health*. ACS Publications.
- Grell, G. A., Peckham, S. E., Schmitz, R., McKeen, S. A., Frost, G., Skamarock, W. C., & Eder,  
415 B. 2005. Fully coupled “online” chemistry within the WRF model. *Atmospheric Environment*, *39*, 6957–6975.
- Guenther, A., Karl, T., Harley, P., Wiedinmyer, C., Palmer, P., & Geron, C. (2006). Estimates of global terrestrial isoprene emissions using MEGAN (Model of Emissions of Gases and Aerosols from Nature). *Atmospheric Chemistry and Physics*, *6*, 3181–3210.
- 420 Gutzwiller, L., Arens, F., Baltensperger, U., Gäggeler, H. W., & Ammann, M. (2002). Significance of semivolatile diesel exhaust organics for secondary HONO formation. *Environmental Science & Technology*, *36*, 677–682.
- Hoor, P., Borken-Kleefeld, J., Caro, D., Dessens, O., Endresen, O., Gauss, M., Grewe, V., Hauglustaine, D., Isaksen, I. S., & Jöckel, P. (2009). The impact of traffic emissions on  
425 atmospheric ozone and OH: Results from QUANTIFY. *Atmospheric Chemistry and Physics*, *9*, 3113–3136.
- Huszar, P., Cariolle, D., Paoli, R., Halenka, T., Belda, M., Schlager, H., Miksovsky, J., & Pisoft, P. (2010). Modeling the regional impact of ship emissions on NO<sub>x</sub> and ozone levels over the Eastern Atlantic and Western Europe using ship plume parameterization. *Atmospheric  
430 Chemistry and Physics*, *10*, 6645–6660.
- Kasibhatla, P., Sherwen, T., Evans, M. J., Carpenter, L. J., Reed, C., Alexander, B., Chen, Q., Sulprizio, M. P., Lee, J. D., & Read, K. A. (2018). Global impact of nitrate photolysis in sea-salt aerosol on NO<sub>x</sub>, OH, and O<sub>3</sub> in the marine boundary layer. *Atmospheric Chemistry and Physics*, *18*, 11185–11203.



- 435 Keene, W. C., Khalil, M. A. K., Erickson, D. J. III, McCulloch, A., Graedel, T. E., Lobert, J. M.,  
Aucott, M. L., Gong, S. L., Harper, D. B., & Kleiman, G. (1999). Composite global  
emissions of reactive chlorine from anthropogenic and natural sources: Reactive Chlorine  
Emissions Inventory. *Journal of Geophysical Research: Atmospheres*, *104*, 8429–8440.
- Kim, S., Kim, S.-Y., Lee, M., Shim, H., Wolfe, G., Guenther, A. B., He, A., Hong, Y., & Han, J.  
440 (2015). Impact of isoprene and HONO chemistry on ozone and OVOC formation in a  
semirural South Korean forest. *Atmospheric Chemistry and Physics (Online)*, *15*.
- Kleffmann, J., Gavriloaiei, T., Hofzumahaus, A., Holland, F., Koppmann, R., Rupp, L.,  
Schlosser, E., Siese, M., & Wahner, A. (2005). Daytime formation of nitrous acid: A  
major source of OH radicals in a forest. *Geophysical Research Letters*, *32*.
- 445 Kurtenbach, R., Becker, K., Gomes, J., Kleffmann, J., Lörzer, J., Spittler, M., Wiesen, P.,  
Ackermann, R., Geyer, A., & Platt, U. (2001). Investigations of emissions and  
heterogeneous formation of HONO in a road traffic tunnel. *Atmospheric Environment*,  
*35*, 3385–3394.
- Lawrence, M. G., & Crutzen, P. J. (1999). Influence of NO<sub>x</sub> emissions from ships on  
450 tropospheric photochemistry and climate. *Nature*, *402*, 167–170.
- Li, M., Zhang, Q., Kurokawa, J.-I., Woo, J.-H., He, K., Lu, Z., Ohara, T., Song, Y., Streets, D.  
G., & Carmichael, G. R. (2017). MIX: A mosaic Asian anthropogenic emission inventory  
under the international collaboration framework of the MICS-Asia and HTAP.  
*Atmospheric Chemistry and Physics (Online)*, *17*.
- 455 Li, Q., Zhang, L., Wang, T., Tham, Y. J., Ahmadov, R., Xue, L., Zhang, Q., & Zheng, J. (2016).  
Impacts of heterogeneous uptake of dinitrogen pentoxide and chlorine activation on  
ozone and reactive nitrogen partitioning: Improvement and application of the WRF-Chem  
model in southern China. *Atmospheric Chemistry and Physics*, *16*, 14875–14890.
- Liu, H., Fu, M., Jin, X., Shang, Y., Shindell, D., Faluvegi, G., Shindell, C., & He, K. (2016).  
460 Health and climate impacts of ocean-going vessels in East Asia. *Nature Climate Change*,  
*6*, 1037–1041.
- Liu, H., Jin, X., Wu, L., Wang, X., Fu, M., Lv, Z., Morawska, L., Huang, F., & He, K. (2018).  
The impact of marine shipping and its DECA control on air quality in the Pearl River  
Delta, China. *Science of the Total Environment*, *625*, 1476–1485.



- 465 Lv, Z., Liu, H., Ying, Q., Fu, M., Meng, Z., Wang, Y., Wei, W., Gong, H., & He, K. (2018).  
Impacts of shipping emissions on PM<sub>2.5</sub> pollution in China. *Atmospheric Chemistry &  
Physics*, 18.
- McDuffie, E. E., Smith, S. J., O'Rourke, P., Tibrewal, K., Venkataraman, C., Marais, E. A.,  
Zheng, B., Crippa, M., Brauer, M., & Martin, R. V. (2020). A global anthropogenic  
470 emission inventory of atmospheric pollutants from sector- and fuel-specific sources  
(1970–2017): An application of the Community Emissions Data System (CEDS). *Earth  
System Science Data Discussions*, 1–49.
- Meusel, H., Kuhn, U., Reiffs, A., Mallik, C., Harder, H., Martinez, M., Schuladen, J., Bohn, B.,  
Parchatka, U., & Crowley, J. N. (2016). Daytime formation of nitrous acid at a coastal  
475 remote site in Cyprus indicating a common ground source of atmospheric HONO and  
NO. *Atmospheric Chemistry and Physics*, 16, 14475–14493.
- Moldanová, J., Fridell, E., Popovicheva, O., Demirdjian, B., Tishkova, V., Faccinnetto, A., &  
Focsa, C. (2009). Characterisation of particulate matter and gaseous emissions from a  
large ship diesel engine. *Atmospheric Environment*, 43, 2632–2641.
- 480 Monge, M. E., D'anna, B., Mazri, L., Giroir-Fendler, A., Ammann, M., Donaldson, D., &  
George, C. (2010). Light changes the atmospheric reactivity of soot. *Proceedings of the  
National Academy of Sciences*, 107, 6605–6609.
- Ndour, M., D'Anna, B., George, C., Ka, O., Balkanski, Y., Kleffmann, J., Stemmler, K., &  
Ammann, M. (2008). Photoenhanced uptake of NO<sub>2</sub> on mineral dust: Laboratory  
485 experiments and model simulations. *Geophysical Research Letters*, 35.
- Osthoff, H. D., Roberts, J. M., Ravishankara, A., Williams, E. J., Lerner, B. M., Sommariva, R.,  
Bates, T. S., Coffman, D., Quinn, P. K., & Dibb, J. E. (2008). High levels of nitryl  
chloride in the polluted subtropical marine boundary layer. *Nature Geoscience*, 1, 324.
- Sarwar, G., Simon, H., Xing, J., & Mathur, R. (2014). Importance of tropospheric ClNO<sub>2</sub>  
490 chemistry across the Northern Hemisphere. *Geophysical Research Letters*, 41, 4050–  
4058.
- Simon, H., Kimura, Y., McGaughey, G., Allen, D., Brown, S., Osthoff, H., Roberts, J., Byun, D.,  
& Lee, D. (2009). Modeling the impact of ClNO<sub>2</sub> on ozone formation in the Houston  
area. *Journal of Geophysical Research: Atmospheres*, 114.

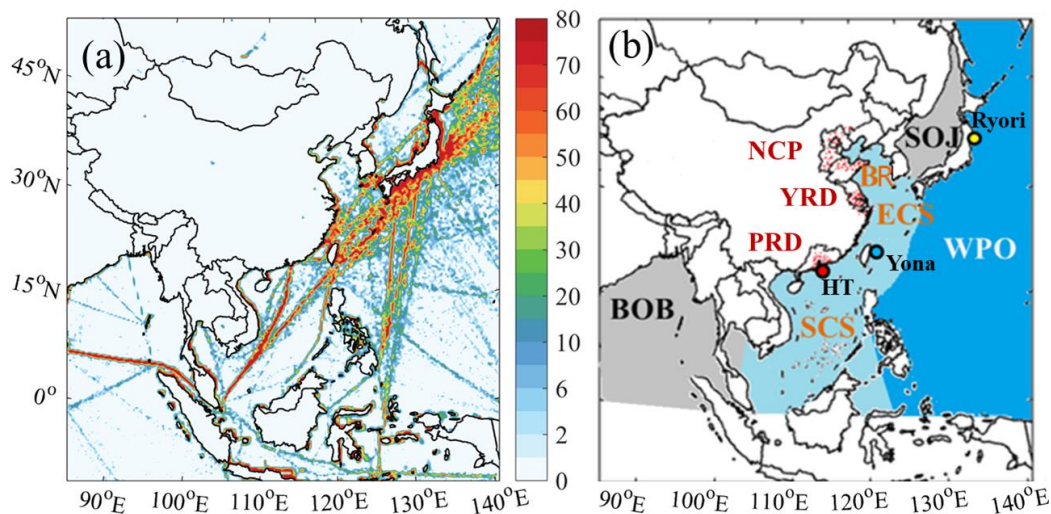


- 495 Song, S.-K., Shon, Z.-H., Kim, Y.-K., Kang, Y.-H., Oh, I.-B., & Jung, C.-H. (2010). Influence of  
ship emissions on ozone concentrations around coastal areas during summer season.  
*Atmospheric Environment*, *44*, 713–723.
- Sun, L., Chen, T., Jiang, Y., Zhou, Y., Sheng, L., Lin, J., Li, J., Dong, C., Wang, C., & Wang, X.  
(2020). Ship emission of nitrous acid (HONO) and its impacts on the marine atmospheric  
500 oxidation chemistry. *Science of The Total Environment*, 139355.
- Takeuchi, M., Miyazaki, Y., Tsunoda, H., & Tanaka, H. (2013). Atmospheric acid gases in  
Tokushima, Japan, monitored with parallel plate wet denuder coupled ion  
chromatograph. *Analytical Sciences*, *29*, 165–168.
- Tham, Y. J., Yan, C., Xue, L., Zha, Q., Wang, X., & Wang, T. (2014). Presence of high nityl  
505 chloride in Asian coastal environment and its impact on atmospheric photochemistry.  
*Chinese Science Bulletin*, *59*, 356–359.
- UNCTAD. (2019). *Review of Maritime Transport*. United Nations Publication, 28.
- Wang, R., Tie, X., Li, G., Zhao, S., Long, X., Johansson, L., & An, Z. (2019). Effect of ship  
emissions on O<sub>3</sub> in the Yangtze River Delta region of China: Analysis of WRF-Chem  
510 modeling. *Science of the Total Environment*, *683*, 360–370.
- Wang, T., Tham, Y. J., Xue, L., Li, Q., Zha, Q., Wang, Z., Poon, S. C., Dubé, W. P., Blake, D.  
R., & Louie, P. K. (2016). Observations of nityl chloride and modeling its source and  
effect on ozone in the planetary boundary layer of southern China. *Journal of  
Geophysical Research: Atmospheres*, *121*, 2476–2489.
- 515 Wen, L., Chen, T., Zheng, P., Wu, L., Wang, X., Mellouki, A., Xue, L., & Wang, W. (2019).  
Nitrous acid in marine boundary layer over eastern Bohai Sea, China: Characteristics,  
sources, and implications. *Science of the Total Environment*, *670*, 282–291.
- Ye, C., Zhang, N., Gao, H., & Zhou, X. (2017). Photolysis of particulate nitrate as a source of  
HONO and NO<sub>x</sub>. *Environmental Science & Technology*, *51*, 6849–6856.
- 520 Ye, C., Zhou, X., Pu, D., Stutz, J., Festa, J., Spolaor, M., Tsai, C., Cantrell, C., Mauldin, R. L., &  
Campos, T. (2016). Rapid cycling of reactive nitrogen in the marine boundary layer.  
*Nature*, *532*, 489–491.
- Zaveri, R. A., & Peters, L. K. (1999). A new lumped structure photochemical mechanism for  
large-scale applications. *Journal of Geophysical Research: Atmospheres*, *104*, 30387–  
525 30415.



- Zha, Q., Xue, L., Wang, T., Xu, Z., Yeung, C., Louie, P. K., & Luk, C. W. (2014). Large conversion rates of NO<sub>2</sub> to HNO<sub>2</sub> observed in air masses from the South China Sea: Evidence of strong production at sea surface? *Geophysical Research Letters*, *41*, 7710–7715.
- 530 Zhang, L., Li, Q., Wang, T., Ahmadov, R., Zhang, Q., Li, M., & Lv, M. (2017a). Combined impacts of nitrous acid and nitryl chloride on lower-tropospheric ozone: New module development in WRF-Chem and application to China. *Atmospheric Chemistry & Physics*, *17*, 9733–9750.
- Zhang, Y., Wen, X. Y., Wang, K., Vijayaraghavan, K., & Jacobson, M. Z. (2009). Probing into  
535 regional O<sub>3</sub> and particulate matter pollution in the United States: 2. An examination of formation mechanisms through a process analysis technique and sensitivity study. *Journal of Geophysical Research: Atmospheres*, 114.
- Zhang, Y., Yang, X., Brown, R., Yang, L., Morawska, L., Ristovski, Z., Fu, Q., & Huang, C. (2017b). Shipping emissions and their impacts on air quality in China. *Science of the  
540 Total Environment*, *581*, 186–198.

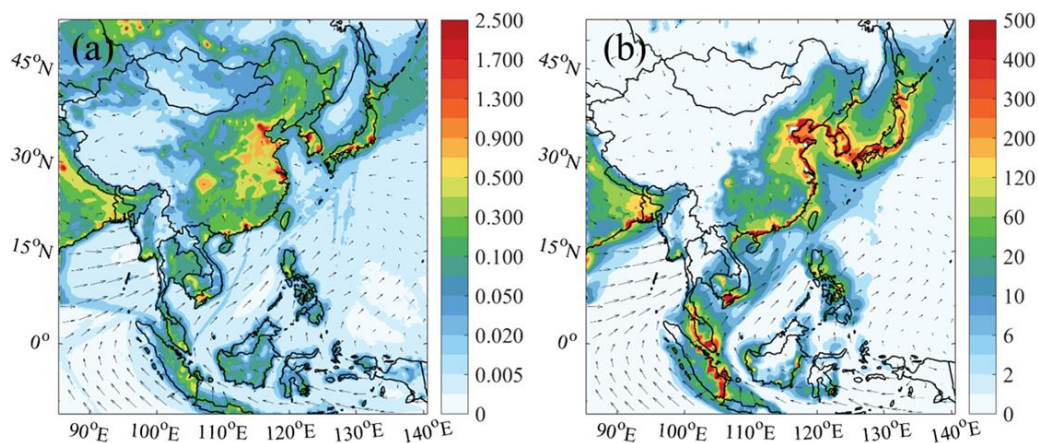
545



550 **Figure 1: (a)  $\text{NO}_x$  emission fluxes from ships (Unit:  $\text{g m}^{-2} \text{ month}^{-1}$ ) in July 2017. (b) Model**  
**domains with six water zones (South China Sea (SCS), East China Sea (ECS), Bohai rim**  
**(BR), Sea of Japan (SOJ), Bay of Bengal (BOB), and West Pacific Ocean (WPO)), three**  
**coastal city clusters (Pearl River Delta (PRD), Yangtze River Delta (YRD) and North**  
**Central Plain (NCP)), and three maritime observational sites (Hok Tsui (HT),**  
555 **Yonagunijima (Yona), and Ryori). Red dots in PRD, YRD, and NCP represent selected**  
**coastal sites. Ranges of latitude and longitude in each body of water are listed in Table S1**  
**in the supplementary information.**

560

565



570 **Figure 2: Spatial distributions of the simulation of average (a) HONO (Unit: ppbv) and (b)**  
**nighttime ClNO<sub>2</sub> (Unit: pptv, 18:00 – 06:00 Local Standard Time (LST)) at the surface**  
**layer (~30 m) in July 2018 from the BASE case. Arrows present simulated wind vectors**  
**from the BASE case.**

575

580

585

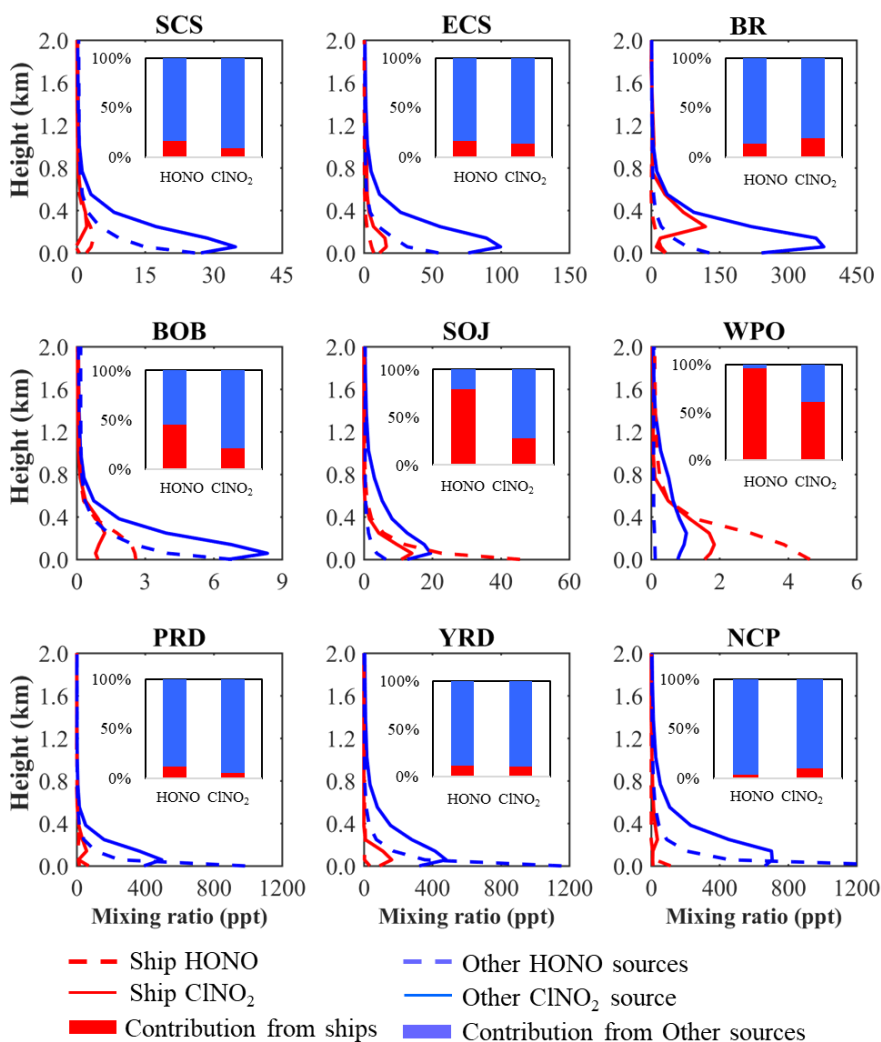
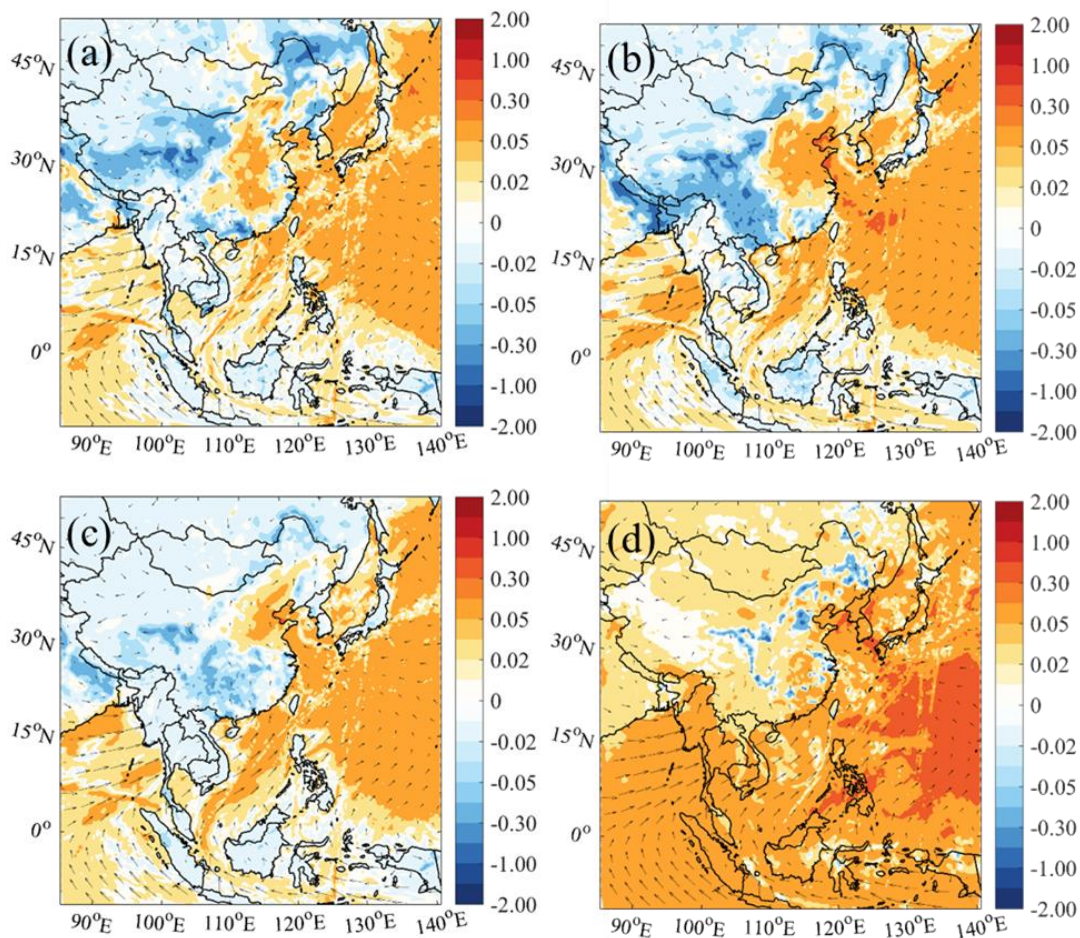


**Figure 3: Vertical profiles of simulated HONO and nighttime CINO<sub>2</sub> (Unit: pptv) from ship emissions and other sources in nine regions. Also shown are contributions of ship emissions and other sources to average HONO and nighttime CINO<sub>2</sub> levels in the marine boundary layer (within 600 m).**

590



595 **Figure 4: Average daytime RO<sub>x</sub> variations (06:00-18:00 LST; Unit: pptv) with (a) default**  
**chemistry (Def-Def\_noship), (b) default and additional HONO chemistry (HONO-**  
**HONO\_noship), (c) default and additional chlorine chemistry (Cl-Cl\_noship), and (d)**  
**default and combined HONO and chlorine chemistry (BASE-BASE\_noship). Arrows**  
**present simulated wind vectors from BASE case.**

600

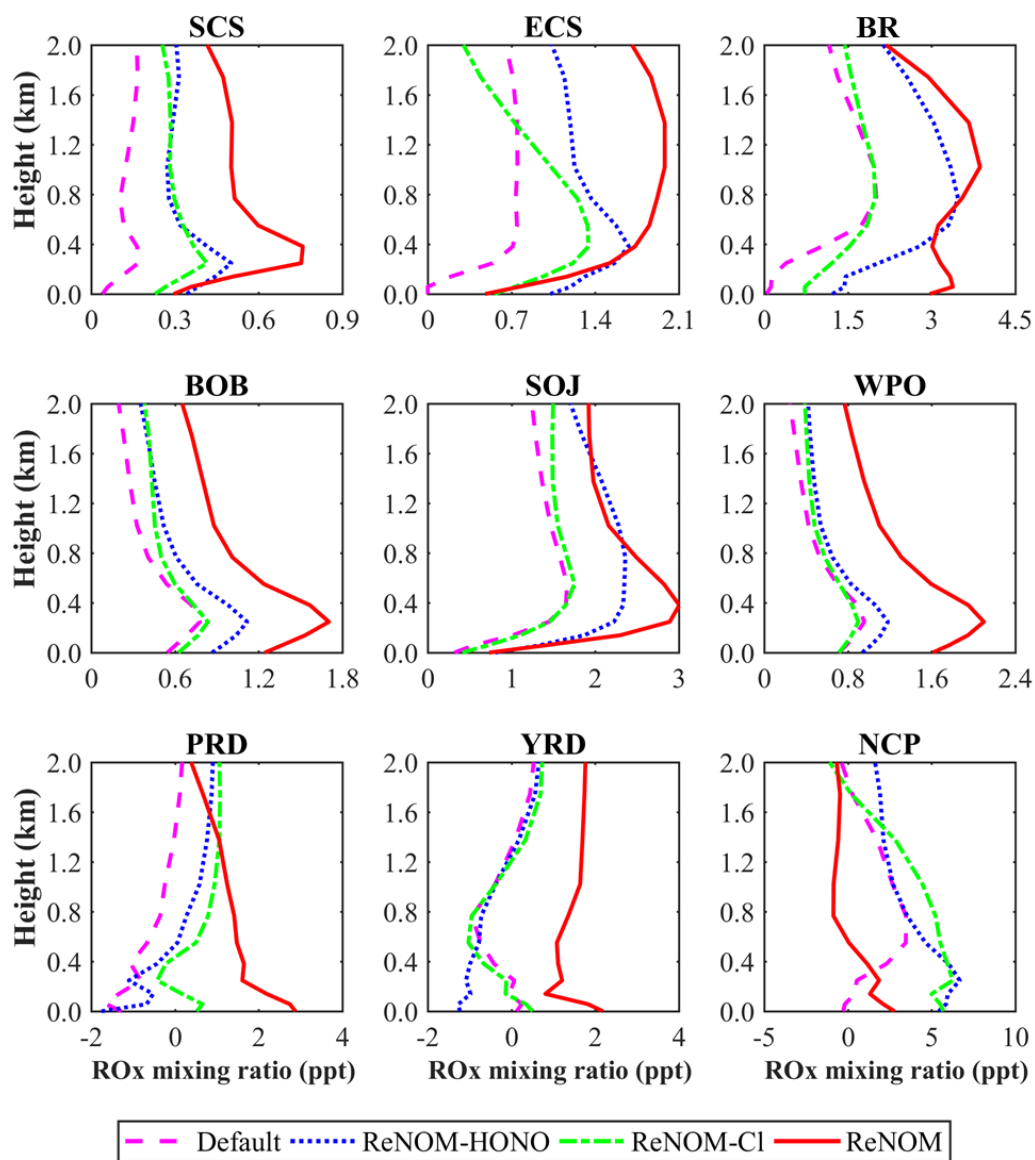
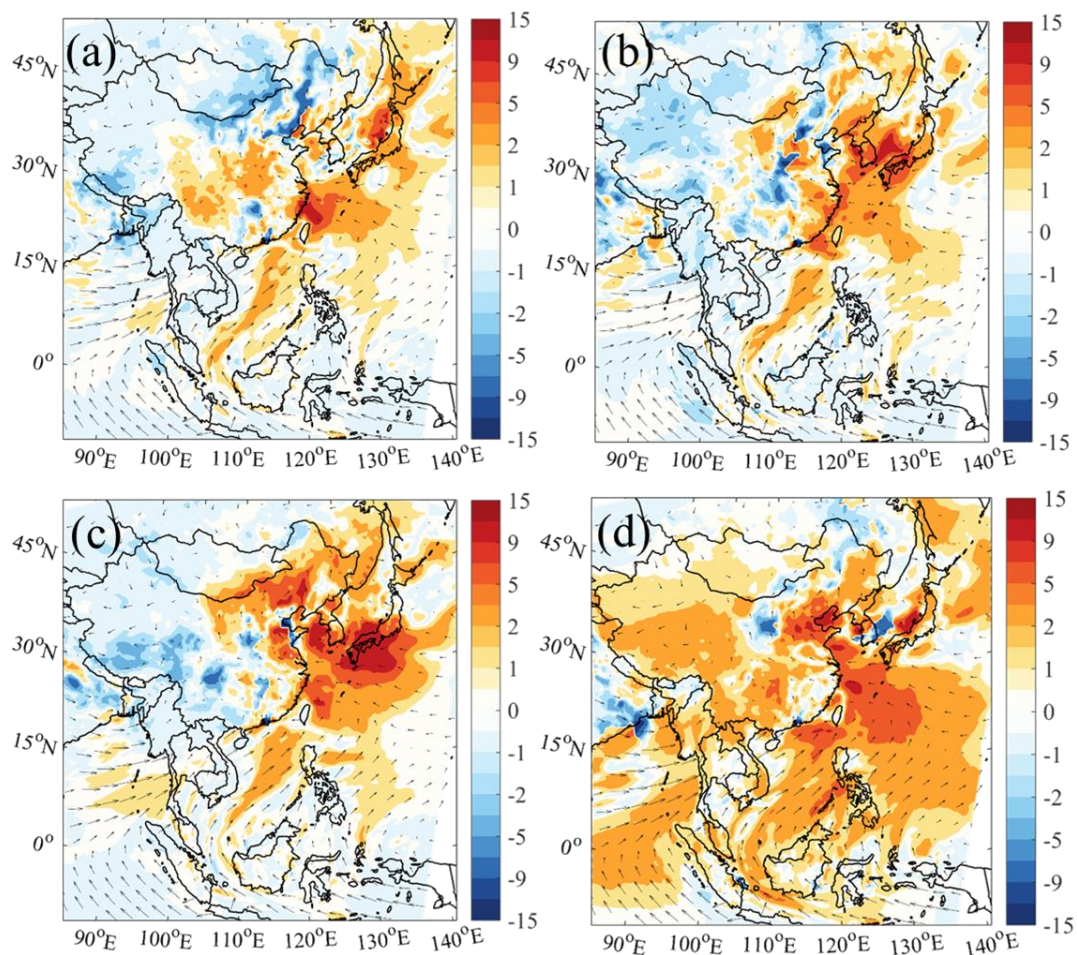


Figure 5: Vertical profiles of daytime RO<sub>x</sub> variations (Unit: pptv) from different chemistry in nine regions.



605

**Figure 6:** This figure is the same as Figure 4 but for average ozone variations (Unit: ppbv).

610

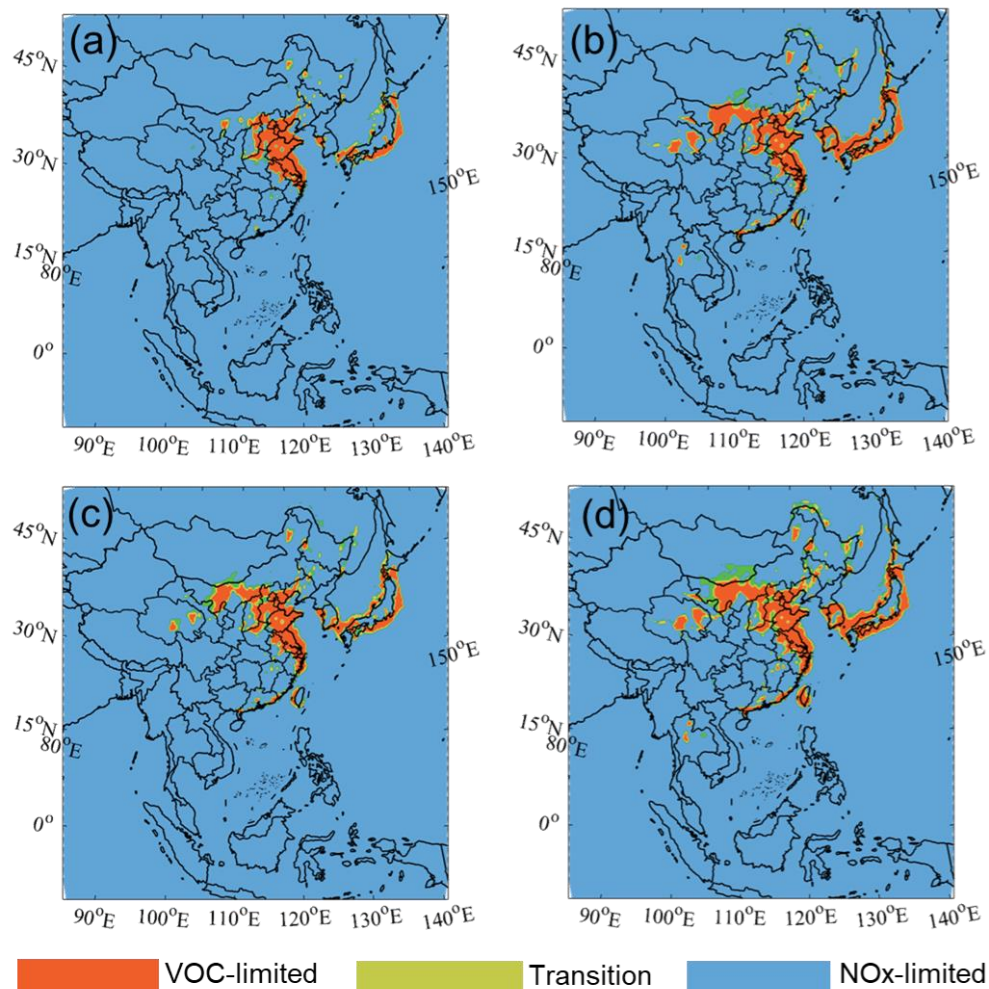
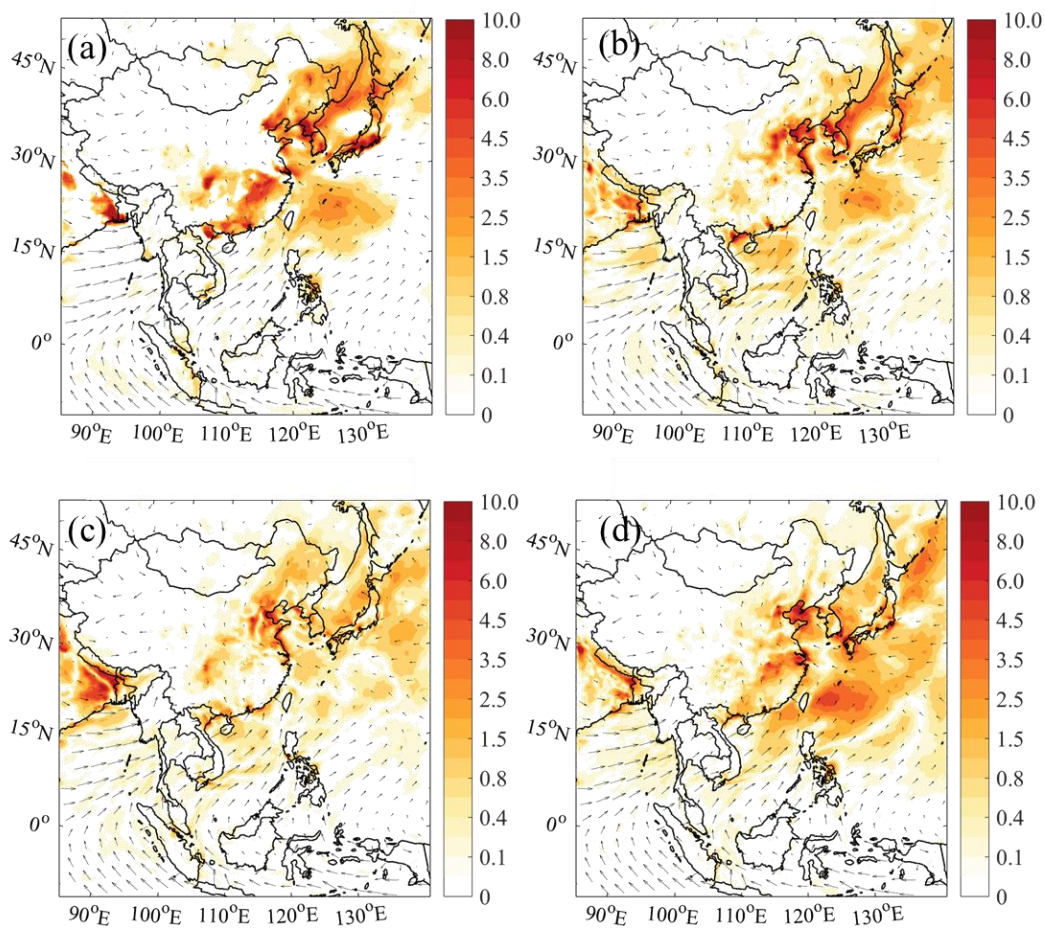
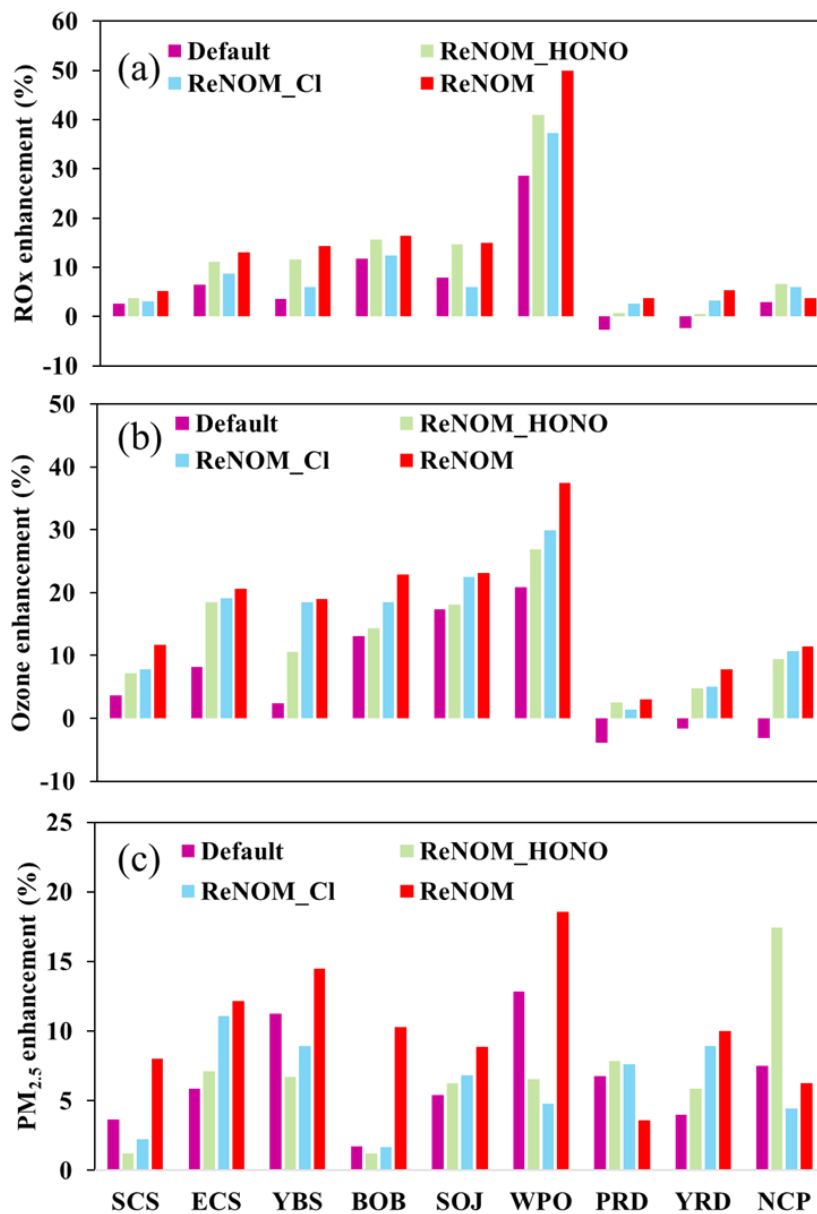


**Figure 7: O<sub>3</sub> sensitivity regimes using (a) Def, (b) HONO, (c) Cl, and (d) Base cases. Classification of ozone sensitivity regime is based on production rates of H<sub>2</sub>O<sub>2</sub> to HNO<sub>3</sub>, and P<sub>H<sub>2</sub>O<sub>2</sub>}/P<sub>HNO<sub>3</sub> of <0.06, 0.06 to 0.2, and >0.2 correspond to VOC-limited, transition, and NO<sub>x</sub>-limited conditions, respectively (Zhang et al., 2009).</sub></sub>**

615



620 **Figure 8:** This figure is the same as Figure 4 but for average  $\text{PM}_{2.5}$  enhancements (Unit:  $\mu\text{g m}^{-3}$ ).



625

**Figure 9:** Contributions of ship emissions with different chemistry to average mixing ratios of (a) daytime RO<sub>x</sub>, (b) ozone, and (c) PM<sub>2.5</sub> (with ship case (i.e., Def) – no ship case (i.e., Def\_noship)) / with ship case (i.e., Def).



630

**Table 1: Experimental Setting**

Cases	Anth Emis <sup>a</sup>	Ship Emis <sup>b</sup>	HONO Chem <sup>c</sup>	Chlorine Chem <sup>d</sup>
Def	Yes	Yes	No	No
Def_noship	Yes	No	No	No
Cl	Yes	Yes	No	Yes
Cl_noship	Yes	No	No	Yes
HONO	Yes	Yes	Yes	No
HONO_noship	Yes	No	Yes	No
BASE	Yes	Yes	Yes	Yes
BASE_noship	Yes	No	Yes	Yes

635

<sup>a</sup> Anthropogenic emissions except for ship emissions.

<sup>b</sup> Ship emissions except for directly emitted HONO.

<sup>c</sup> HONO chemistry.

<sup>d</sup> Chlorine chemistry.

640